Biocatalysis and Agricultural Biotechnology 21 (2019) 101354

Contents lists available at ScienceDirect

Biocatalysis and Agricultural Biotechnology

journal homepage: http://www.elsevier.com/locate/bab

Green synthesis of iron oxide nanoparticles using *Terminalia bellirica* and *Moringa oleifera* fruit and leaf extracts: Antioxidant, antibacterial and thermoacoustic properties

Gautham B. Jegadeesan *, K. Srimathi, N. Santosh Srinivas, S. Manishkanna, D. Vignesh

School of Chemical and Biotechnology, SASTRA Deemed To Be University, Thanjavur, 613401, India

ARTICLE INFO

Keywords:
Biogenic Fe
Antioxidant
Antimicrobial
Thermal conductivity
Nanofluid
Terminalia bellirica
Moringa oleifera

ABSTRACT

This study presents a facile biogenic synthesis of iron (Fe) NPs using aqueous extracts of three plant sources: *Terminalia bellirica* (TB); *Moringa oleifera* fruit (MOF) and *Moringa oleifera* leaves (MOL). The total phenolic content was highest for TB extract (3581.36 ± 2.38 μg/ml equivalent of gallic acid). The synthesized Fe NPs were characterized using UV–Vis spectroscopy, Fourier Transform Infrared Spectroscopy (FT-IR), Scanning Electron Microscopy (SEM), Transmission Electron Microscopy (TEM) and X-Ray Diffraction (XRD). FT-IR spectra of the extracts and nanosuspensions were similar, with peaks observed at around 3300–3400 cm^{-1}, 1600 cm^{-1}, 1050–1150 cm^{-1} and 500 cm^{-1}, corresponding to O–H, C═O, C–O and C–H stretching, indicating the participation of biomolecules in the nanomaterial synthesis process. TEM and SEM images show single spherical particles for T-Fe (21.32 nm), and irregular shaped MOF-Fe and MOL-Fe (particle size of 45 nm). XRD analysis confirmed the presence of hematite (α-Fe_2O_3) and ferric oxyhydroxide (FeOOH) in the Fe NPs. The antioxidant activity of the aqueous extracts was higher than that of the biogenic Fe NPs, with TB extract the highest among all, given its higher phenolic content. The antimicrobial activity of Fe-NPs was higher than the extract alone, with T-Fe and MOL-Fe the most potent towards *S. aureus* and *B. subtilis*. The thermal conductivity of the Fe NPs dispersed in propylene glycol: water base fluid was determined. The high thermal conductivity of Fe NPs in glycol - water mixtures showed its potential as a possible nanofluid for various heat transfer applications.

1. Introduction

Controlling materials at the nano-level can result in the production of nanomaterials with improved properties and functionalities. As a result, nanotechnology is revolutionizing our ability to tackle problems in the medical, manufacturing, chemical, military, space exploration, human hygiene, energy production, water purification and other fields (Wiesner et al., 2006; Sharma et al., 2019). Over the last decade, the use of nanoparticles (NPs) in semiconductor devices, solar cells, cosmetics, catalytic reactions, protein adsorption, textiles, computer transistors, nanofluids and biomedical applications like biomarkers, biosensors, diagnostic and prognostic devices has risen significantly (Bhatia, 2016; Ferrari, 2005; Leena et al., 2015; Qu et al., 2013; Wiesner et al., 2006; Sharma et al., 2019; Kamran et al., 2019). Typically, nanoparticles are produced using chemical or hydrothermal, which involves the use of toxic chemicals (Akhtar et al., 2013; G Ingale, 2013; Herlekar et al., 2014; Kamran et al., 2019). However, with increasing focus on the development of green synthesis methods, toxic chemicals are being replaced by plant extracts (Akhtar et al., 2013; G Ingale, 2013; Herlekar et al., 2014; Saif et al., 2016; Radini et al., 2018; Bashir et al., 2019; Kamran et al., 2019). Due to the cost-effective, safe and non-toxic method for NP synthesis, and the ability of plant extracts to act as capping/stabilizing agents thus reducing particle size and improving reactivity, green synthesis methods are preferred (Saif et al., 2016; Radini et al., 2018; Bashir et al., 2019; Kamran et al., 2019).

Plant extracts are shown to produce more stable metal nanoparticles and are more amenable to large scale production of NPs as compared to microorganisms (Saif et al., 2016; Radini et al., 2018; Bashir et al., 2019; Kamran et al., 2019). The plant extracts contain biomolecules such as flavanoids, terpenoids, and other polyphenols which coat the NP surface, preventing agglomeration, and thus help obtain an uniform particle size distribution (Mittal et al., 2013; Saif et al., 2016; Vaseghi et al., 2017; Radini et al., 2018; Bashir et al., 2019; Kamran et al., 2019; Gunarani et al., 2019). Several nanomaterials such as Ag NPs, Cu and

* Corresponding author.
E-mail address: jegadeesan@scbt.sastra.edu (G.B. Jegadeesan).

https://doi.org/10.1016/j.bcab.2019.101354
Received 4 August 2019; Received in revised form 17 September 2019; Accepted 22 September 2019
Available online 23 September 2019
1878-8181/© 2019 Elsevier Ltd. All rights reserved.

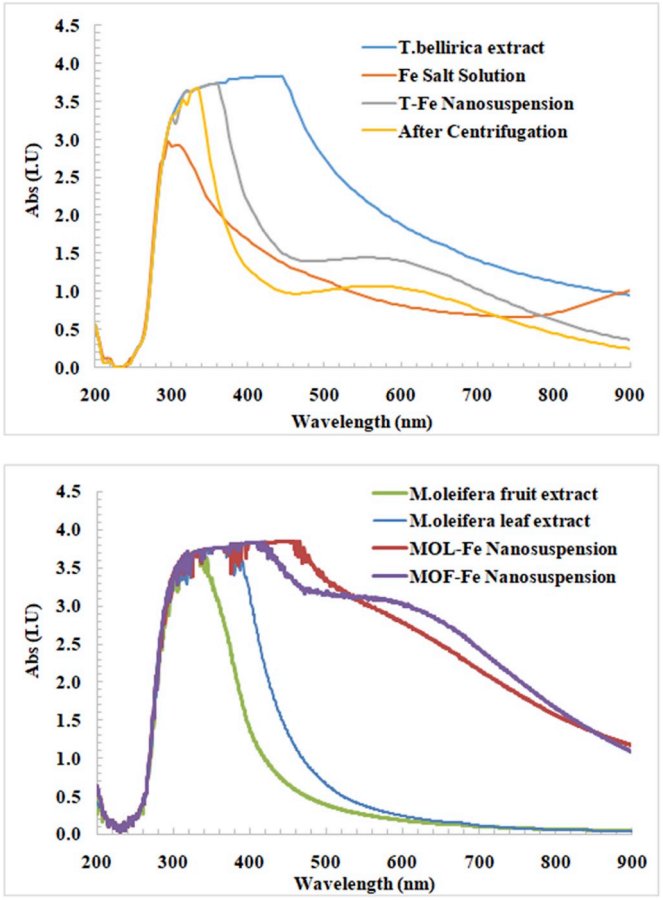

Fig. 1. UV–Vis absorption spectra for the extract and the Fe NP suspensions prepared using *T. bellirica, M. oleifera* fruit and *M. oleifera* leaf extracts.

CuO NPs, FeO and Fe_3O_4 NPs have been synthesized biologically using fungi, bacteria and plant extracts for a variety of applications (Akhtar et al., 2013; G Ingale, 2013; Herlekar et al., 2014; Saif et al., 2016; Radini et al., 2018; Bashir et al., 2019; Kamran et al., 2019; Nandhini et al., 2019). Biogenic Fe NPs have been synthesized using plant extracts (Schröfel et al., 2014; Vijayaraghavan and Ashokkumar, 2017; Rajiv et al., 2017; Bashir et al., 2019), bacteria (Moon et al., 2010), fungi (Bharde et al., 2006), and algae such as *Chlorococcum sp.* (Subramaniyam et al., 2015).

In our previous studies (Gunarani et al., 2019), we have reported the use of biogenic Fe NPs for heavy metal removal and dye degradation. With increasing use of Fe NPs as drug delivery carriers (Arruebo et al., 2007; Schröfel et al., 2014), it is also important to determine their antioxidant and antimicrobial capabilities. In recent years, use of Fe/Fe-oxide NPs has increased significantly in areas of diagnosis and treatment of disease, electrical components like transformers, and nanofluids (Madhavi et al., 2013; Saif et al., 2016; Mansoori et al., 2008; Radini et al., 2018; Bashir et al., 2019; Kamran et al., 2019). It is also known that if the property of the nanomaterial is tuned well, it can have significant effect on its thermal properties. Nanosuspensions containing 0.5–5 wt% of nanoparticles (Al_2O_3, Fe_2O_3, ZnO, Ag and CuO among others) in base fluids such as ethylene glycol, propylene glycol, water etc, have shown higher thermal conductivity than the base fluid (Ahmadi et al., 2018; Anu and Hemalatha, 2018; Kharat et al., 2019; Leena et al., 2015; Nabeel Rashin and Hemalatha, 2014). Several studies have reported the antioxidant and antibacterial properties of Fe NPs, prepared using plant extracts. However, scant literature was available on Fe NPs synthesized using *Terminalia bellirica, Moringa oleifera* fruit and *Moringa oleifera* leaves as the plant sources for nanoparticles

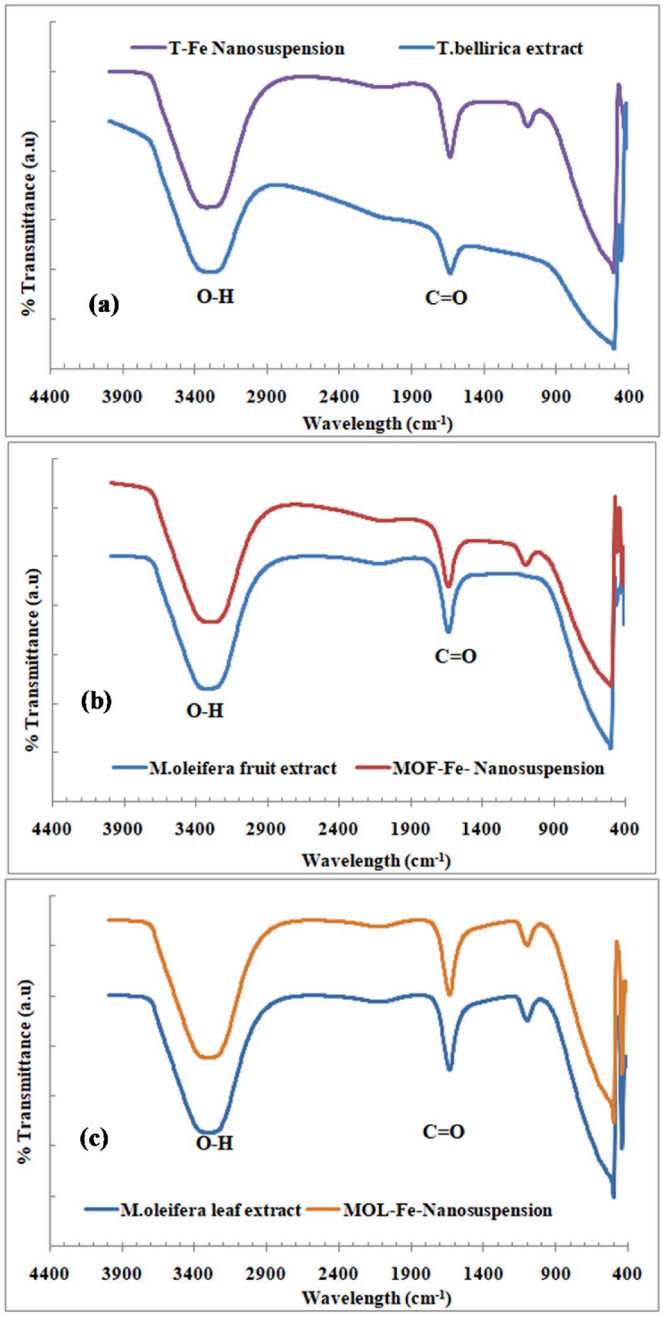

Fig. 2. FT-IR spectra for the extract and the Fe NP suspensions prepared using (a) *T. bellirica,* (b) *M. oleifera* fruit and (c) *M. oleifera* leaf extracts.

preparation. Further, and to the best of our knowledge, there is little work done on the use of biosynthesized Fe NPs as nanofluids. Thus, in this study, we synthesize Fe NPs using aqueous extracts of *Terminalia bellirica* (TB) and; *Moringa oleifera* fruit (MOF) and *Moringa oleifera* leaves (MOL) and report its applicability as an antioxidant, antimicrobial agent and as a nanofluid. *Terminalia bellirica* is a wild fruit, found in the plains of Southern India and used in Ayurvedic formulations. *Moringa oleifera*, also an edible plant, is also commonly used in India for medicinal treatment and also a flocculant for water treatment. The biosynthesized Fe NPs were characterized for their surface morphology, and the antioxidant and anti-microbial properties of the aqueous extracts and extract – mediated Fe NPs were determined. The thermoacoustic properties of the plant extract/water as base fluid and 1 wt% Fe-NPs in the propylene –water mixture as nanofluid suspension was also determined using interferometric techniques. Properties such as

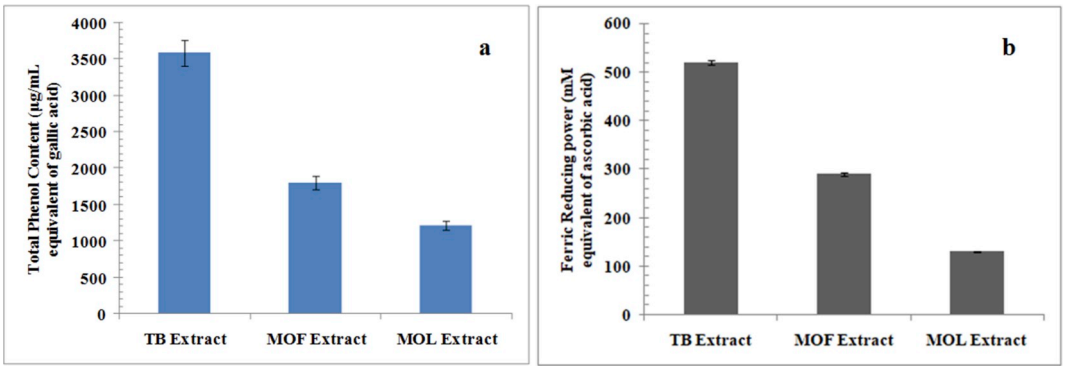

Fig. 3. Biochemical properties of plant extracts (*T. bellirica (TB), M. oleifera fruit (MOF) and M. oleifera leaf (MOL)*). (a) Total phenolic content, (b) Ferric reducing power.

adiabatic compressibility, intermolecular free length, acoustic impedance, and thermal conductivity were calculated from the experimental data.

2. Experimental

2.1. Materials

All the reagents used were of analytical reagent grade with high purity (>99%). Hydrochloric acid (HCl 37%), sodium hydroxide (NaOH), sodium biocarbonate ($NaHCO_3$), Folin-Coicalteau reagent, gallic acid, ferric chloride heptahydrate ($FeCl_2.7H_2O$), potassium ferricyanide ($K_3Fe(CN)_6$), trichloroacetic acid, potassium phosphate, sulphuric acid, sodium phosphate, ammonium molybdate, hydrogen peroxide (30 vol.%) and 2, 2-diphenyl-1-picrylhydrazyl were obtained from Sigma Aldrich (India) and used as received. *Terminalia bellirica* fruit, *Moringa oleifera* fruit and *Moringa oleifera* leaves were purchased from the local market in Thanjavur, India.

2.2. Synthesis of Fe NPs using biogenic methods

Fe NPs were synthesized using biogenic method, as reported in our previous work (Gunarani et al., 2019). Typically, the plant sources (i.e., fruit or leaves) were dried in open atmosphere to remove all moisture content, and then ground to fine size (<1 µm). Extraction using distilled water was performed in reflux mode at a weight ratio of 1:20 solid: liquid for 2 h, and the obtained extract was filtered and stored for NP synthesis. The extracts are denoted as TB (*Terminalia bellirica*), MOF (*Moringa oleifera* fruit) and MOL (*Moringa oleifera* leaves) extracts, henceforth.

Biogenic Fe NPs were synthesized by adding 0.5 M of Fe-salt to the aqueous plant extract drop-wise in a sonicated reactor. Formation of black color NPs indicated the presence of iron. The Fe NPs synthesized are denoted as T-Fe (using *T. bellirica* extract), MOF-Fe (using *M. oleifera* fruit extract) and MOL-Fe (using *M. oleifera* leaves extract), henceforth. The plant extracts and Fe-NPs were characterized using UV–Vis absorption spectrophotometer (Hach, India), scanning electron microscope (SEM, JSM 6701F, JEOL, Japan), transmission electron microscope (TEM, Hitachi), x-ray diffraction with Cu Kα radiation of wavelength 1.5408 Å (XRD, D8 Focus, Bruker, Germany), energy dispersive x-ray spectroscopy (EDAX, Hitachi), and fourier transform – infra red spectroscopy (FTIR, Nicolet, ThermoFisher).

2.3. Estimation of total phenolic content and ferric reducing powder of plant extracts

The total phenolic content of the extracts was determined by using the method reported elsewhere (Singleton et al., 1999; Bashir et al., 2019; Kamran et al., 2019). 200 µl of the extract was mixed with 2 ml of 5% $NaHCO_3$ solution. 500 µl of Folin-Coicalteau reagent was added to this and the mixture was incubated in dark at room temperature for 30 min. The absorbance was measured at 720 nm, with gallic acid as standard. The final phenolic content of the extracts were expressed in terms of gallic acid equivalents (GAE). The ferric reducing power of the extracts was determined by using the methods reported in literature (Benzie and Strain, 1996; Bashir et al., 2019; Kamran et al., 2019). 2.5 ml of the extract was mixed with 2.5 ml of phosphate buffer (0.2 M, pH = 6.6). 2.5 ml of 1% potassium ferricyanide solution was added and the mixture was incubated at 50 °C for 20 min. After cooling, 2.5 ml of 10% trichloroacetic acid was added to the mixture. The mixture was centrifuged at 8000 rpm for 10 min 5 ml of supernatant was taken, and 5 ml of 0.1% ferric chloride solution was added. The absorbance was measured at 700 nm, with ascorbic acid as standard, and the reducing power was expressed in terms of ascorbic acid. The tests were performed in triplicates and results were recorded as mean ± SD.

2.4. Estimation of the antioxidant activity of plant extracts and biogenic Fe NPs

The anti oxidant activity of the extracts and nanoparticle suspensions were evaluated using phosphomolybdate assay, 2,2-diphenyl-1-picryl-hydrazyl (DPPH) free radical assay and hydrogen peroxide scavenging assay (Saeed et al., 2012; Mirza et al., 2018). Aqueous suspensions of the nanoparticles and extracts were used for the study. For the phosphomolybdate assay, 1 mL aliquot of sample was mixed with 10 ml of phosphomolybate reagent (0.6 M sulphuric acid, 28 mM sodium phosphate, 4 mM ammonium molybdate). The mixture was incubated at 95 °C for 90 min. After cooling down the mixture, the absorbance was measured at 695 nm, with ascorbic acid as the standard. The final anti oxidant activity of the extracts were expressed in terms of ascorbic acid equivalents. The DPPH (2, 2-diphenyl-1-picrylhydrazyl) free radical scavenging capacity of the extracts and nanoparticles were determined by adding 100 µl of the sample to 3.9 ml of a solution of 0.025 g/l DPPH –methanol suspension. The mixture was incubated in 25 °C for 30 min. The absorbance was then measured at 515 nm. Ascorbic acid was used as positive control. Methanol was also used as control to determine the decrease in the absorbance of the samples. The scavenging activity of DPPH was reported in terms of percentage basis as shown below (equation (1)):

$$\%\ DPPH\ scavenged = \frac{(A_{control} - A_{sample})*100}{A_{control}} \quad (1)$$

The hydrogen peroxide scavenging activity of the extract was determined by adding 1 ml of the sample with 9 ml of 100 mM hydrogen peroxide solution made in phosphate buffer (0.2 M, pH 7.0). After incubating the mixture in room temperature for 30 min, the absorbance was measured at 277 nm. Distilled water was used as the control. The scavenging of hydrogen peroxide was reported in percentage basis

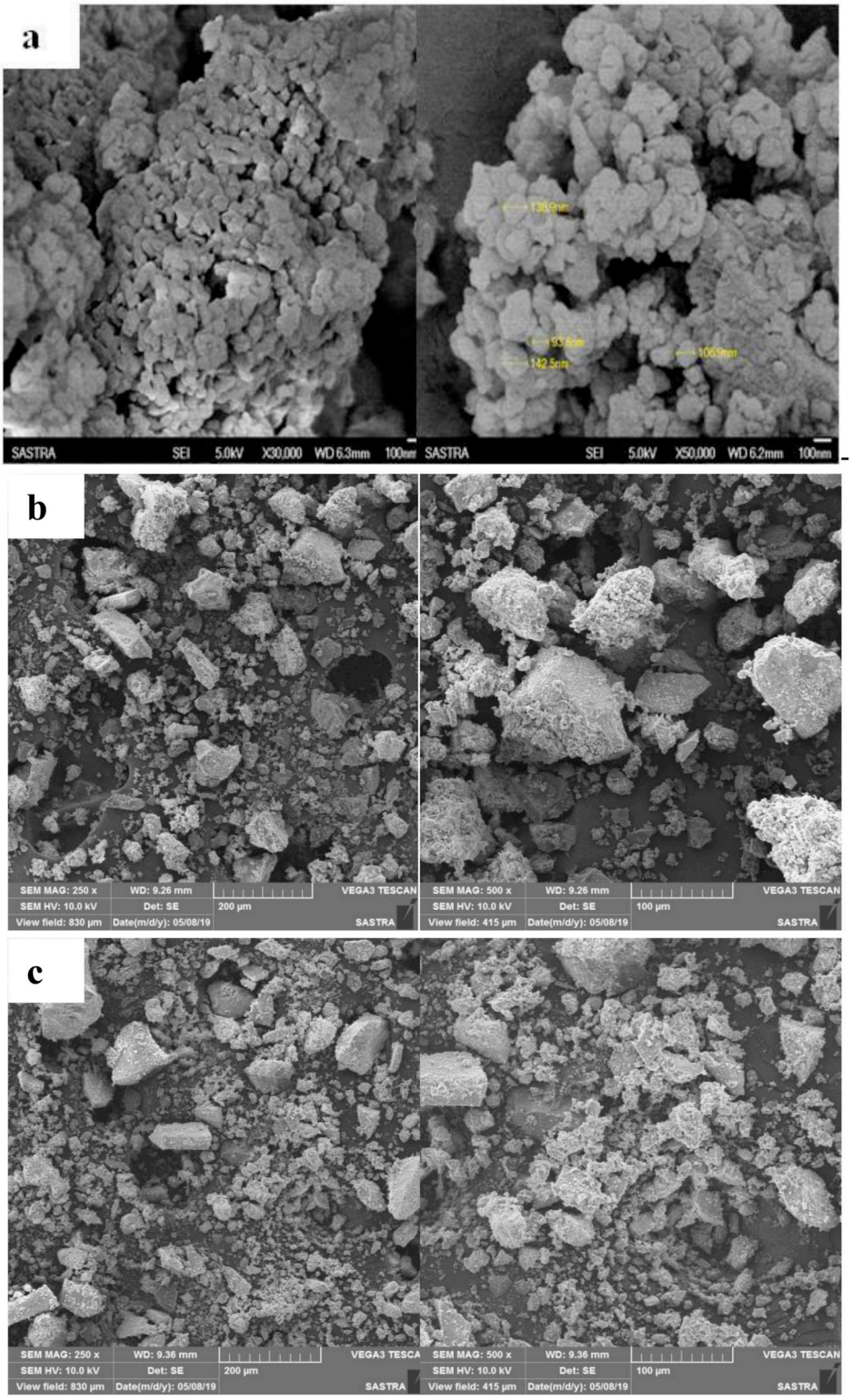

Fig. 4. Scanning Electron Microscopic (SEM) images of Fe NPs prepared using (a) *T. bellirica,* (b) *M. oleifera* fruit and (c) *M. oleifera* leaf extracts.

(equation (2)). The tests were performed in triplicates and results were recorded as mean ± SD.

$$\%\ H_2O_2\ scavenged = \frac{(A_{control} - A_{sample})*100}{A_{control}} \quad (2)$$

2.5. Estimation of the antimicrobial activity of plant extracts and biogenic Fe NPs

The antimicrobial activity of the extracts and Fe NPs was determined using the well diffusion methods (Naseem and Farrukh, 2015; Mirza et al., 2018; Bashir et al., 2019; Kamran et al., 2019). The microorganisms chosen for this study were: *Escherichia coli* (MTCC 443),

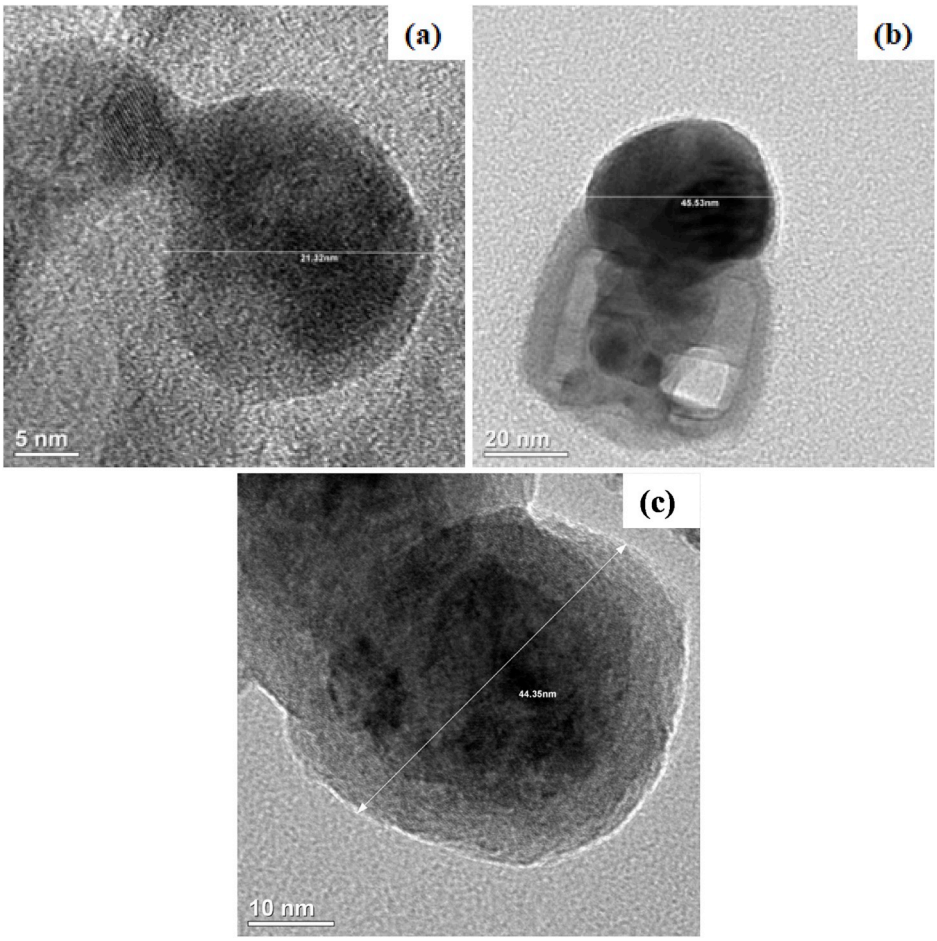

Fig. 5. Transmission Electron Microscopic (TEM) images of Fe NPs prepared using (a) *T. bellirica,* (b) *M. oleifera* fruit and (c) *M. oleifera* leaf extracts.

Table 1
EDAX spectral analysis of the nanoparticles.

Element	Weight %		
	T-Fe	M-Fe	MK-Fe
Carbon (C)	53.76	42.43	48.52
Oxygen (O)	42.14	45.45	44.51
Iron (Fe)	4.1	7.08	5.17
Sulphur (S)	–	3.83	1.80
Potassium (K)	–	1.21	–

Staphylococcus aureus (MTCC 96), *Bacillus subtilis* (MTCC 441), *Pseudomonas aeruginosa* (MTCC 1688) (Kumar et al., 2018). The bacterial strains were grown in nutrient broth at 37 °C and were maintained on nutrient agar (NA) slants. The bacterial (~1×10^8 colony forming units (CFU)/ml) was uniformly spread on the surface of the nutrient agar plates using sterile cotton swabs. After the solidification of the media, the cultures were swabbed on the plates. Wells of 6 mm diameter were bored using a sterile 1 ml tip. 20 µl of the samples and plant extracts and Fe NP suspensions were loaded in each well. The plates were incubated at 37 °C for 24 h and the zone of inhibition was measured (Kumar et al., 2018; Sivamaruthi et al., 2019). The tests were performed in triplicates and results were recorded as mean ± SD.

2.6. Determination of thermal conductivity of Fe NP - nanofluids

Ultrasonic velocity has become an effective diagnostic parameter for understanding the behavior of fluids, and determining their thermodynamic properties (Anu and Hemalatha, 2018; Leena et al., 2015). Measurement of ultrasonic velocity provides an insight into the molecular interactions between the solute and solvent, and in the case of nanofluid suspension, their thermal conductivities. The ultrasonic velocity of the base fluid and the nanofluid suspensions were measured using a nanofluid ultrasonic interferometer (Mittal Enterprises, India) operating at 2 MHz, at 298 K and 1 atm pressure. Typically, nanoparticles are dispersed in glycol – water mixtures and the thermal conductivity of the base fluid (glycol – water) and the nanofluid (base fluid with the nanoparticles) are determined. In this study, propylene glycol (PG) – water mixture was used as the base fluid (Anu and Hemalatha, 2018), and 1 wt% of the Fe NPs were dispersed in the base fluid of various mixtures. The nanofluid was sonicated for 1 h to disperse the particles in the nanofluid and improve its stability. The change in velocity with vol. fraction of the solute in the solute-solvent mixture was determined and used to calculate thermo-acoustic parameters: adiabatic compressibility, intermolecular free length, acoustic impedance, and thermal conductivity using known correlations (Anu and Hemalatha, 2018; Nabeel Rashin and Hemalatha, 2014). The density was determined using a specific gravity bottle by the relative measurement method. The tests were replicated six times and results were recorded as mean ± SD.

3. Results and discussion

3.1. UV–Vis and FT-IR spectra of plant extracts and the biogenic Fe NPs

The aqueous extracts of the three different plant sources (i.e., *Terminalia bellirica*, *Moringa oleifera* fruit and *Moringa oleifera* leaf) and the Fe NPs synthesized using the extracts, were characterized for their

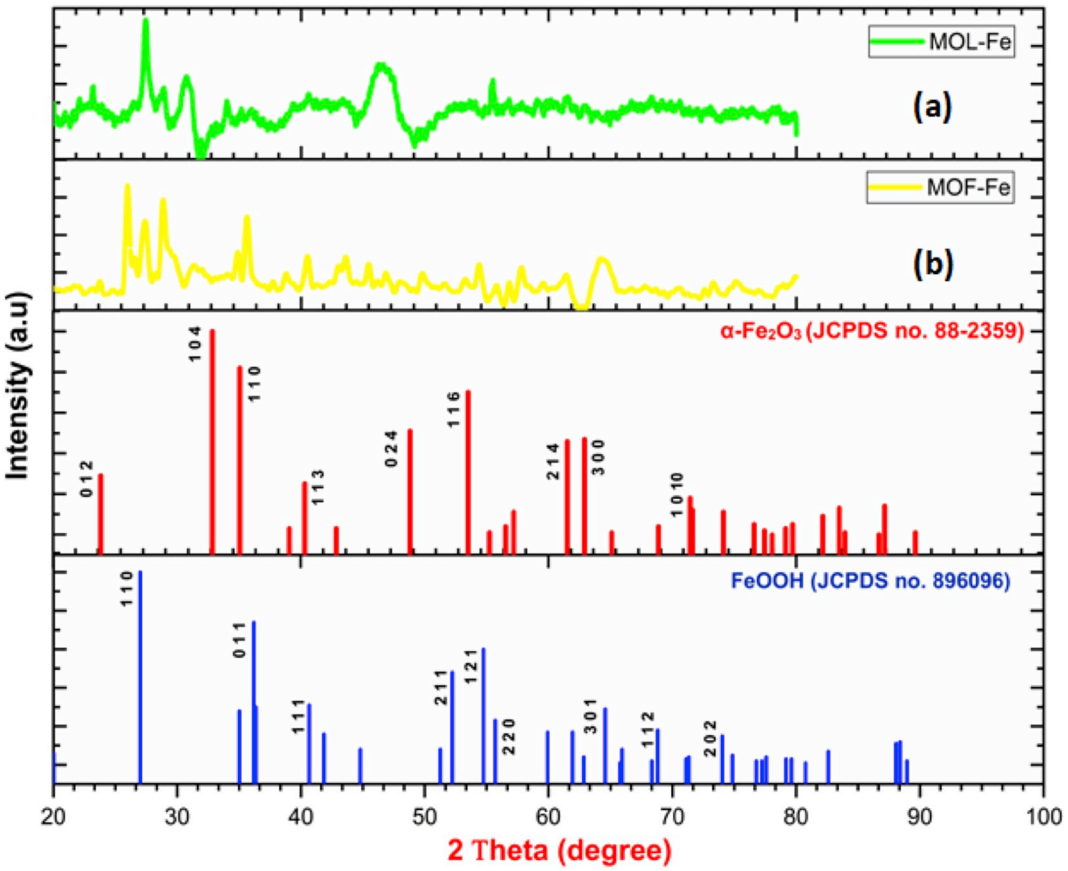

Fig. 6. X-ray diffraction (XRD) of Fe NPs prepared using (a) *M. oleifera* leaf (MOL-Fe) and (b) *M. oleifera* fruit (MOF-Fe) extracts.

properties. Fig. 1 shows the UV–Vis absorption spectra for the extract and the Fe NP suspension. The absorption spectra of the extracts (i.e., TB, MOF and MOL) were all similar, a broad maximum observed between the wavelength ranges of 300–600 nm. Fe-salt solution showed a peak at 300 nm, and the Fe NPs showed peaks at around 400 nm. The nanosuspension of Fe NPs also exhibited the same spectra at 300 nm, indicating the presence of Fe-NPs in the suspension. Mirza et al. (2018) reported the UV–Vis absorbance spectra of *Agrewia optiva* and *Prunus persica* extract around 200 nm and the extract-mediated iron oxide nanoparticles peaks at about 270–280 nm. Vasantharaj et al. (2019) and Rajiv et al. (2017) reported the presence of peaks attributable to Fe NPs at 405 nm. Peaks observed at 600 nm were indicative of the precipitated solids, mostly due to the formation of Fe NPs (Harshiny et al., 2015; Vasantharaj et al., 2019).

Fig. 2 (a, b, c) shows the FT-IR spectra for the extracts and the nanosuspensions. The FT-IR spectra of the extract are almost similar, with peaks observed at around 3300–3400 cm^{-1}, 1600 cm^{-1}, 1050–1150 cm^{-1} and 500 cm^{-1}, and similar to previous studies (Edison and Sethuraman, 2012; Sneha and Karthikeyan, 2019). The FT-IR spectra of Fe NPs nanosuspension were also similar, with one additional peak at around 1100 cm^{-1}. The peak obtained around 3300 cm^{-1} is due to the vibrations of O–H stretching (indicative of the presence of alcohols/phenolic groups). The peak obtained around 1600 cm^{-1} is due to the vibrations of C═O stretching suggesting the presence of carboxylic acids. The peaks from 1050–1150 cm^{-1} and 500 cm^{-1} were indicated the presence of Fe–O. Adio et al. (2017) synthesized Fe NPs using *Aloe vera* plant and attributed peak at 1100 cm^{-1} and 500 cm^{-1} to Fe–OH and Fe–O, respectively. The presence of the biomolecules in Fe NPs confirmed the stabilizing role played by them in the synthesis of the nanoparticles. In several studies, the FT-IR spectra of plant extracts showed the presence of peaks at around 2700 cm^{-1} (O–H stretching) and 2300 cm^{-1} (N–H) (Ibraheem et al., 2019; Saif et al., 2016). The absence of these specific peaks is due to the type of plant, season and extraction method.

3.2. Biochemical properties of the plant extracts

The total phenolic content, measured as gallic acid equivalent was found to be the highest for (TB) extract, 3581.36 ± 2.38 μg/ml equivalent of gallic acid or 3.5 g/kg, as seen in Fig. 3a. This is several orders of magnitude lower than the total amount of polyphenols present in *T. bellirica* fruit. Pfundstein et al. (2010) reported that the total polyphenols content in *T.bellirica* fruit was 223. 7 g/kg. The higher value obtained in their study was due to the use of methanolic extracts of the fruit. The total phenolic content of the *M. oleifera* fruit (MOF) and *M. oleifera* leaves (MOL) extracts was 2 to 3 fold lower than in TB extracts. The ferric reducing power of TB extract was significantly higher (519.9 ± 0.004 mM equivalent of ascorbic acid) than MOF and MOL extracts, having ferric reducing power of 289.9 ± 0.004 and 130.7 ± 0.003 mM equivalent of ascorbic acid, respectively. This resulted correlated with the data on TB extract having the maximum phenolic content and therefore the maximum ferric reducing power. It was also observed that the extract with the higher reducing power gave the maximum yield of Fe NPs and also the highest percent of Fe in the Fe NPs. Reduction in the total phenolic content in the extract was observed, post synthesis, which indicated the participation of the polyphenols in the process.

3.3. Characterization of the biogenic Fe NPs

The Fe NPs synthesized were characterized using energy dispersive x-ray spectroscopy (EDAX), scanning electron microscopy (SEM), transmission electron microscopy (TEM) and x-ray diffraction (XRD). SEM images in Fig. 4 showed mostly spherical particles for T-Fe NPs

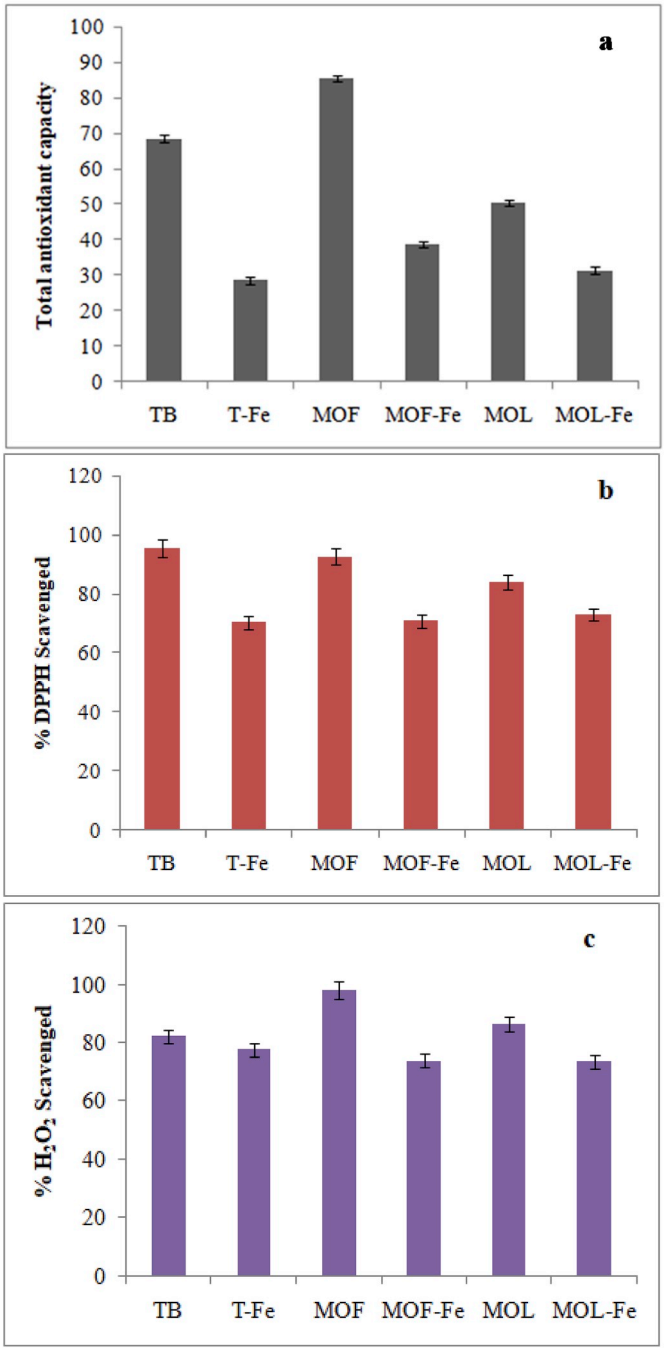

Fig. 7. Antioxidant properties of the plant extracts (*T. bellirica (TB), M. oleifera fruit (MOF) and M. oleifera leaf (MOL)*) and the Fe NPs synthesized using the extracts (*T. bellirica (T-Fe), M. oleifera (MOF-Fe) and M. oleifera leaf (MOL-Fe)*) using (a) phosphomolybdate assay (expressed as μg/mL of ascorbic acid equivalents (AAE)), (b) DPPH scavenging assay and; (c) hydrogen peroxide scavenging assay.

with size ranging from 140 nm to 300 nm. The NPs sizes sythesized from *M. oleifera* fruit (MOF) and *M. oleifera* were almost similar in size and surface morphology, but non-spherical. TEM images show single spherical particles for T-Fe with particle size of 21.32 nm (Fig. 5). The particle size for MOF-Fe and MOL-Fe were higher, about 45 nm. Mirza et al. (2018) reported the size of *Agrewia optiva* and *Prunus persica* extract mediated Fe–O NPs to be in the range of 10–70 nm. Fe NPs synthesized using *Aloe vera* plant and *R. tuberosa* extracts was about 20–80 nm in size (Adio et al., 2017; Vasantharaj et al., 2019), similar to the data obtained here. EDAX analysis showed that Fe content in the NPs synthesized using

Table 2
Zone of inhibition (mean of three replicates ± SD, in mm) of plant extracts (*T. bellirica (TB), M. oleifera fruit (MOF) and M. oleifera leaf (MOL)*) and the Fe NPs synthesized using the extracts (*T. bellirica (T-Fe), M. oleifera (MOF-Fe) and M. oleifera leaf (MOL-Fe)*) against *E. coli*; *P. aeruginosa*; *S. aureus*; *B. subtilis*.

Microorganism	*E.coli*	*P. aeruginosa*	*S aureus*	*B subtilis*
Extracts				
TB	Nil	Nil	Nil	Nil
MOF	Nil	Nil	Nil	Nil
MOL	Nil	Nil	Nil	Nil
Biogenic Fe-NPs				
T-Fe	12.5 ± 1	12 ± 1.5	15 ± 2	14 ± 1
MOF-Fe	13 ± 1.5	11 ± 1	13 ± 1	12 ± 2
MOL-Fe	12 ± 1.5	14 ± 2.5	15 ± 1	15 ± 1.5

the extracts ranged from 4-7 wt percent, with M-Fe NPs having the highest Fe content (Table 1). The percent composition of C and O was observed to be higher in the T-Fe NPs (53% and 42% respectively), when compared to that in MOF-Fe and MOL-Fe NPs (in which C and O ranged from 42-48 wt%). The high percent of carbon – oxygen molecules in the T-Fe sample indicated the presence of residual biomolecules on the Fe NPs surface. Previous studies have also reported the presence of carbon-oxygen in the biosynthesized Fe-NPs (Adio et al., 2017; Jagathesan and Rajiv, 2018; Vasantharaj et al., 2019).

The raw XRD data was analyzed using FullProf Suite and the significant crystal phases was identified. The crystallize size was determined using the Debye-Schrerrer formulae:

$$d = \frac{K\lambda}{\beta cos\theta} \quad (3)$$

where d is the mean size of crystallites (nm), K is crystallite shape factor a good approximation is 0.9, λ is the X-ray wavelength, β is the full width at half the maximum (FWHM) in radians of the X-ray diffraction peak and θ is the Braggs' angle (deg.). In our previous study (Gunarani et al., 2019), we had reported that T-Fe NPs were primarily composed of Fe_2O_3 with diffraction peaks corresponding to indices (2 2 0) and (2 0 0). X-ray diffraction analysis of MOF-Fe and MOL-Fe also indicated the presence of hematite (Fe_2O_3 or α – Fe_2O_3) nanoparticles and iron oxyhydroxides (FeOOH) (Fig. 6). Diffraction patterns for MOF-Fe major peaks at 2θ of 26° and 28.5°, corresponding to Fe_2O_3 (2 1 1) and FeOOH (1 1 0), respectively. Smaller peaks at 35.6° corresponded to the (1 1 0) indices of α – Fe_2O_3. XRD pattern for MOL-Fe showed major peak at 28.5° corresponding to FeOOH (1 1 0), with minor peaks at 23.2° (0 1 2 of α – Fe_2O_3). Biosynthesized iron oxide nanoparticles using *Agrewia optiva* and *Prunus persica* extracts were reported to be Fe_3O_4 (Mirza et al., 2018). Other studies have reported presence of α – Fe_2O_3 with (2 2 0) and (1 1 0) indices and smaller amounts of β – Fe_2O_3 in the biosynthesized Fe NPs (Ahmmad et al., 2013; Bishnoi et al., 2018; Makarov et al., 2014). Similar patterns were also observed in Fe NPs synthesized using *Terminalia chebula* aqueous extract (Saif et al., 2016) and eucalyptus leaf extracts (Wang et al., 2014). Using the Braggs' angle of 28.5° (corresponding to the (1 1 0) indices of FeOOH) in the Deby Schrerrer formulae, the crystal size for the Fe-NPs, was: MOL-Fe (30.5 nm); MOF-Fe (37.3 nm); T-Fe (40.88 nm), and was similar to the sizes obtained from TEM images. Presence of broad peaks at 2θ = 27° can be attributed to the presence of organic molecules (corresponding to peaks of C with indices 1 1 0), consistent with FTIR results.

3.4. Antioxidant properties of the extract and the biogenic Fe NPs

The antioxidant ability of the extracts and the Fe NPs was determined using phosphomolybdate assay (Fig. 7a), DPPH free-radical scavenging assay (Fig. 7b) and the hydrogen peroxide scavenging assay (Fig. 7c). The total antioxidant capacity of the extracts and the extracted mediated Fe NPs are expressed as μg/mL of ascorbic acid equivalents (AAE). In general, the antioxidant activity of the aqueous plant extracts was higher

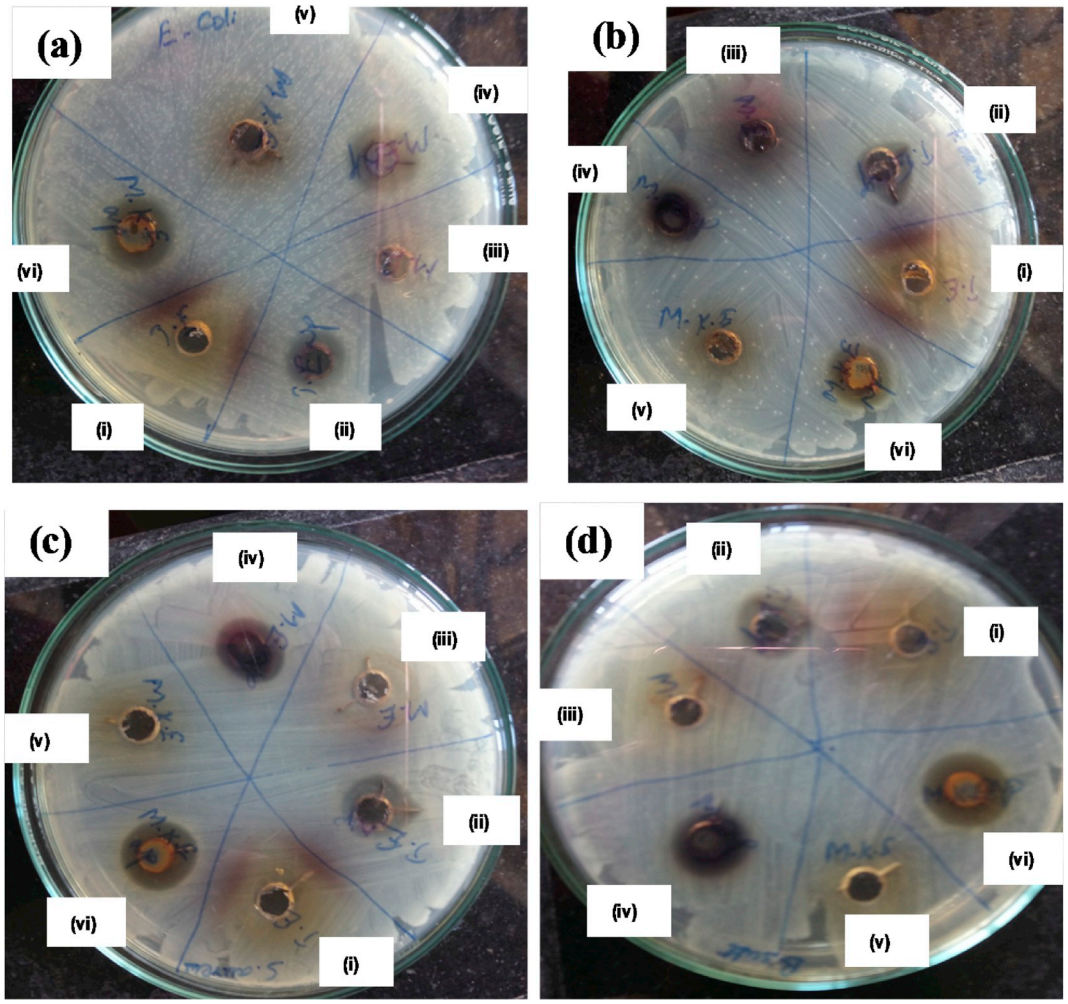

Fig. 8. Growth inhibition of common microorganisms caused by plant extracts (*T. bellirica (TB), M. oleifera fruit (MOF) and M. oleifera leaf (MOL)*) and the Fe NPs synthesized using the extracts (*T. bellirica (T-Fe), M. oleifera (MOF-Fe) and M. oleifera leaf (MOL-Fe)*) - (a) *E. coli*; (b) *P. aeruginosa*; (c) *S. aureus*; (d) *B. subtilis* (i) TB; (ii) T-Fe (iii) MOF; (iv) MOF-Fe; (v) MOL; (vi) MOL-Fe.

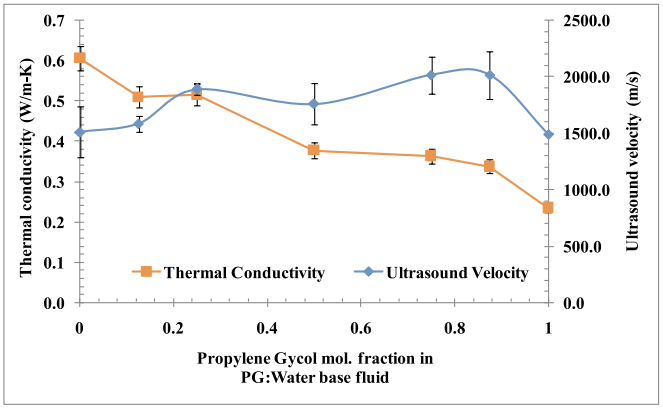

Fig. 9. Ultrasound velocity and thermal conductivity of propylene glycol (PG) – water base fluid at various mixtures.

than that of the biogenic Fe NPs. Among the plant extracts, TB extracts had higher antioxidant activity than MOF and MOL extracts (i.e., *M. oleifera extracts)* given its higher phenolic content. The reduced antioxidant activity of the biogenic Fe NPs is largely due to the reduced concentration of the plant molecules in the nanoparticle suspensions, when compared to the original plant extracts (Muthukumar and Matheswaran, 2015; Vasantharaj et al., 2019). Chemically synthesized Fe NPs showed near-zero antioxidant activity, therefore, the anti-oxidant nature of the biogenic Fe NPs is largely due to the bio-molecules covering the core of the Fe shell. Among the Fe NPs, T-Fe had better antioxidant activity when compared to MOF-Fe and MOL-Fe. Minor variation observed in the antioxidant activity among the Fe NPs might be due to differences in size, % biomolecules presence in the core, and the type of biomolecules present.

3.5. Anti-microbial properties of the extract and the biogenic Fe NPs

The anti-bacterial properties of the extracts and the Fe NPs was determined using *E. coli*, *S. aureus*, *B. subtilis*, *P. aeruginosa* as the microorganism in well diffusion assay using plant extract: water volume ratio at 1:10. Table 2 presents the zone of inhibition for the extracts and the Fe NPs. The observation of the zone of inhibition in the agar plates clearly indicated the antimicrobial properties of the Fe NPs (Fig. 8). It was interesting to note that none of the plant extracts showed any noticeable zone of inhibition in well diffusion assay. Hence, it can be inferred that they do not possess any anti bacterial activity against the chosen microorganisms. It has been previously reported that methanolic extracts had higher anti-micrcobial activity that plant extract (Vasantharaj et al., 2019). All the biogenic Fe NPs possessed antimicrobial activity towards the chosen microorganisms. Activity against microorganisms occurs due to the small size of the iron oxide nanoparticles

Table 3
Thermo-acoustic properties of the base fluid: propylene glycol (PG) – water mixture at various molar ratios.

PG mol fraction	Water mol fraction.	Acoustic Impedance (Z x 10^6) (kg $m^{-2}s^{-1}$)	Adiabatic compressibility β x 10^{-10} (N^{-1} m^2)	Intermolecular Free Length (Å)	Thermal Conductivity (W/m-k)
0	1	1.51	4.39	4.55	0.61
0.125	0.875	1.59	3.95	4.10	0.51
0.25	0.75	1.91	2.77	2.88	0.51
0.5	0.5	1.80	3.17	3.28	0.38
0.75	0.25	2.08	2.39	2.48	0.36
0.875	0.125	2.08	2.39	2.48	0.34
1	0	1.55	4.33	4.49	0.23

Table 4
Thermo-acoustic properties of plant extracts (*T. bellirica (TB), M. oleifera fruit (MOF) and M. oleifera leaf (MOL)*).

Extract	Average Velocity (m s^{-1})	Density (kg m^{-3})	Acoustic Impedance (Z x 10^6) (kg $m^{-2}s^{-1}$)	Adiabatic compressibility β x 10^{-10} (N^{-1} m^2)	Intermolecular Free Length (Å)	Thermal Conductivity (W/m-k)
TB	1184 ± 87.6	783	0.927	9.11	9.45	0.40
MOF	1193 ± 58.9	776	0.926	9.05	9.39	0.40
MOL	1160 ± 71.5	773	0.897	9.61	9.97	0.39

Table 5
Thermo-acoustic properties of Fe NPs dispersed in PG – water base fluid.

PG mol fraction	Water mol fraction.	Average Velocity (m/s)	Acoustic Impedance (Z x 10^6) (kg $m^{-2}s^{-1}$)	Adiabatic compressibility β x 10^{-10} (N^{-1} m^2)	Intermolecular Free Length (Å)
T-Fe NPs					
0.2	0.8	1616 ± 111.7	1.44	4.31	4.47
0.4	0.6	1693 ± 41.3	1.59	3.72	3.86
0.6	0.4	1680 ± 40	1.64	3.64	3.77
MOF-Fe NPs					
0.2	0.8	1613 ± 60.2	1.38	4.50	4.67
0.4	0.6	1696 ± 171.1	1.52	3.87	4.02
0.6	0.4	1704 ± 145.9	1.62	3.61	3.75
MOL-Fe NPs					
0.2	0.8	1593 ± 195	1.41	4.46	4.62
0.4	0.6	1696 ± 45.6	1.53	3.85	3.99
0.6	0.4	1576 ± 164	1.54	4.12	4.27

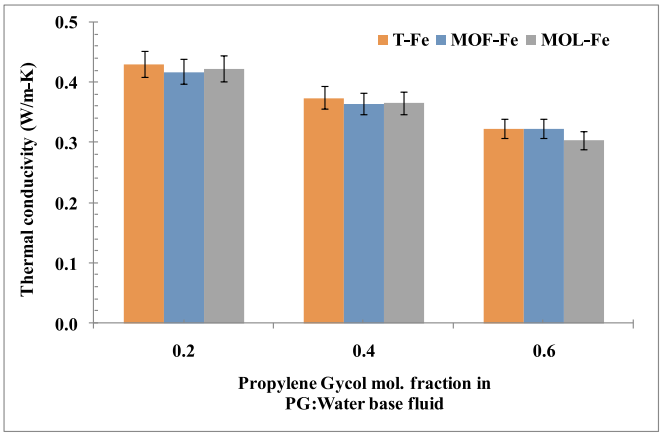

Fig. 10. Thermal conductivity of Fe-NPs in propylene glycol (PG) – water base fluid at various mixtures.

which penetrate into the bacterial cell. Mirza et al. (2018) reported that when the negatively charged microorganism electrostatically interacts with positively charged Fe-oxide NPs, they oxidize and die. Among those, T-Fe and MOL-Fe appeared to be the most potent towards *S. aureus* and *B. subtilis* with the zone of inhibition of 14 and 15 mm, respectively. The zone of inhibition was found to be similar to those reported in earlier studies (Jagathesan and Rajiv, 2018; Mirza et al., 2018; Vasantharaj et al., 2019; Sahoo et al., 2019). Sahoo et al. (2019) reported the antibacterial activity against *E. coli* (15 ± 0.5 mm) followed by *B. subtilis* (13 ± 0.5 mm) and *S. aureus* (12 ± 0.5 mm). The antibacterial activity against *E. coli* was observed by *M. oleifera* seed mediated FeNPs was 6 mm, followed by *M. oleifera* leaves mediated -FeNPs at 5 mm (Katata-Seru et al., 2018). It can also be deduced that increasing the concentration of Fe in the Fe NPs increases the antibacterial potential of the NPs, given the higher Fe percent in T-Fe when compared to MOF-Fe.

3.6. Thermoacoustic characterization of the extracts and Fe NPs

Various correlations have been developed to determine thermal properties of fluids using measured ultrasonic velocities, as it is the quantum of molecular vibration in the fluid, when a wave passes through it (Anu and Hemalatha, 2018; Kharat et al., 2019; Leena et al., 2015; Nabeel Rashin and Hemalatha, 2014). Adiabatic compressibility (β_{ad}) is the decrease of volume per unit increase of sound pressure, without transfer of heat or mass of substance to the surroundings, and is determined using equation (4) in terms of the density of the nanofluid (ρ) and the ultrasonic velocity (*U*):

$$\beta\left(N^{-1}m^{2}\right) = \frac{1}{\rho U^{2}} \quad (4)$$

The acoustic impedance (Z) is calculated as:

$$Z\left(Ns\,m^{-3}\right) = \rho^{*}U \quad (5)$$

The intermolecular free length is the distance covered by the sound wave between adjacent molecules and is a measure of the intermolecular attraction between the components and the solvent. The intermolecular free length (L_f) is calculated as per equation (6a and b) where β_{ad} is the adiabatic compressibility and K_T is the Jacobson constant at specific temperature T (Anu and Hemalatha, 2018; Leena et al., 2015).

$$L_f\ (m) = K_T\sqrt{\beta_{ad}} \tag{6a}$$

$$K_T = (93.875 + 0.345\mathrm{T}) * 10^{-8} \tag{6b}$$

It is a widely accepted theory that hydroacoustic vibrations of the base fluid are responsible for heat transfer in liquid. Based on this theory, Bridgman derived a formula to determine thermal conductivity of pure liquids based on ultrasound velocity, which was later modified for nanofluid suspension to understand the effect of nanoparticles on thermal conductivity of nanofluids. The thermal conductivity of the nanofluid suspensions were calculated as per equation (7a and b), where K_{nf} is the thermal conductivity of the nanofluid in W/m-k; N_A is the Avogadro's constant, V_m is the apparent molar volume of the nanofluid (equation (7b)), K_b is the Boltzmann's constant, M_{np} is the molar mass of nanoparticle, m is the molality of solution, ρ_{bf} and ρ_{nf} are the densities of the base fluid and nanofluids, and U is the ultrasound velocity (Anu and Hemalatha, 2018; Dhondge et al., 2010).

$$K_{nf}\left(\frac{W}{m-K}\right) = 3\left(\frac{N_A}{V_m}\right)^{2/3} K_b * U \tag{7a}$$

$$V_m = \frac{M_{np}}{\rho_{nf}} + \frac{\left[1000*\left(\rho_{bf}-\rho_{nf}\right)\right]}{m\rho_{bf}\rho_{nf}} \tag{7b}$$

Fig. 9 presents the change in ultrasound velocity and thermal conductivity of propylene glycol (PG) – water base fluid at different mixtures. As can be seen in the figure, the ultrasound velocity initially increased with increasing PG content in the base fluid, then reducing for pure PG, similar to the trend reported by Anu et al. (Anu and Hemalatha, 2018). The correlation chosen here correctly predicted the thermal conductivity of water (0.61 W/m-K) and PG (0.23 W/m-K). Table 3 presents the other thermodynamic properties of the base fluid. With increase in PG content in the nanofluid, the intermolecular interactions between PG and water increased, thus reducing the intermolecular free length. Table 4 present the thermodynamic data on the plant extracts alone to see if they can replace PG: water as base fluid. To the best of our knowledge, no one has reported the thermal conductivity of the plant extracts. As seen in Table 4, the thermal conductivity of extracts was about 0.40 W/m-K, and almost similar to a 50:50 PG: water. Higher values of acoustic impedance usually suggest significant interaction between particles and the base fluid molecules, which decreases the intermolecular distance between the molecules therefore causing impedance to ultrasound waves (Anu and Hemalatha, 2018). The lower values for acoustic impedance for the extract suggested insignificant interaction between the polyphenols and water. Nevertheless, the data suggests that plant extracts can replace PG: water as base fluid.

Since the maximum ultrasound velocities for the base fluid (PG-water) were observed for 20:80, 40:60 and 60:40 PG: water ratio, the thermal conductivity of the Fe NPs – nanofluid was determined for these specific ratios of base fluid, similar to other studies reported earlier (Anu and Hemalatha, 2018; Pastoriza-Gallego et al., 2011). Table 5 presents the thermo-acoustic parameters of the Fe NPs – nanofluid, and Fig. 10 shows the thermal conductivity of the nanofluid. As seen in Table 5, the decrease in adiabatic compressibility and free length supports such particle and fluid interaction. The thermal conductivity of Fe-NPs – PG – water nanofluids was about 0.42 W/m-K for PG: water ratio of 0.2:0.8. With increase in PG content in the nanofluid, the thermal conductivity was observed to decrease, largely due to change in density/viscosity of the fluid. Pastoriza et al. (Pastoriza-Gallego et al., 2011) reported the thermal conductivity of Fe_2O_3 – ethylene glycol and Fe_3O_4 – ethylene glycol nanofluids to be in the range of 0.25–0.28 W/m-K. With nearly a 50% increase in thermal conductivity of biosynthesized Fe NPs (also Fe_2O_3) in PG-water mixtures, use of these nanofluids is recommended.

4. Conclusions

The biosynthesis of Fe NPs using tropical plant extracts, *Terminalia bellirica*, *Moringa oleifera* fruit and *Moringa oleifera* leaves is presented. XRD analysis showed that the Fe NPs were mostly Fe_2O_3 and FeOOH, with crystallite size of 35–40 nm. The SEM and TEM images of the Fe NPs showed spherical particles for T-Fe and some non-spherical particles for MOF-Fe and MOL-Fe. FT-IR and UV–Vis absorbance spectra confirmed the participation of the polyphenols in the synthesis process. The Fe NPs synthesized using *Terminalia bellirica* showed better antioxidant activity when compared to the other biosynthesized Fe NPs. T-Fe and MOL-Fe were most potent towards *S. aureus* and *B. subtilis*. The thermal conductivity of the plant extracts was similar to that of a 50:50 propylene glycol: water base fluid, and therefore can be used as a replacement. Data based on the thermo-acoustic properties of Fe NPs showed that biosynthesized Fe NPs had higher thermal conductivity than other Fe-oxide nanofluids. All the results in this study suggest that the biosynthesized iron nanoparticles have excellent antioxidant, antimicrobial and thermal properties.

Acknowledgements

The authors acknowledge the help and support of SASTRA University towards the completion of the work.

Appendix A. Supplementary data

Supplementary data to this article can be found online at https://doi.org/10.1016/j.bcab.2019.101354.

References

Adio, S.O., Omar, M.H., Asif, M., Saleh, T.A., 2017. Arsenic and selenium removal from water using biosynthesized nanoscale zero-valent iron: a factorial design analysis. Process Saf. Environ. Prot. 107, 1301–1518, 527.
Ahmadi, M.H., Tatar, A., Seifaddini, P., Ghazvini, M., Ghasempour, R., Sheremet, M.A., 2018. Thermal conductivity and dynamic viscosity modeling of Fe_2O_3 water nanofluid by applying various connectionist approaches. Numer. Heat Transf. A 74, 1301–1322.
Ahmmad, B., Leonard, K., Shariful Islam, M., Kurawaki, J., Muruganandham, M., Ohkubo, T., Kuroda, Y., 2013. Green synthesis of mesoporous hematite (α- Fe_2O_3) nanoparticles and their photocatalytic activity. Adv. Powder Technol. 24, 160–167.
Akhtar, M.S., Panwar, J., Yun, Y.S., 2013. Biogenic synthesis of metallic nanoparticles by plant extracts. ACS Sustain. Chem. Eng. 1, 591–602.
Anu, K., Hemalatha, J., 2018. Ultrasonic and magnetic investigations of the molecular interactions in zinc doped magnetite Nanofluids. J. Mol. Liq. 256, 213–223.
Arruebo, M., Fernández-Pacheco, R., Ibarra, M.R., Santamaría, J., 2007. Magnetic nanoparticles for drug delivery. Nano Today 2 (3), 22–32.
Bashir, A.K., Mayedwa, N., Kaviyarasu, K., Razanamahandry, L.C., Matinise, N., Bharuth-Ram, K., Tchokonté, M.B.T., Ezema, F., Maaza, M., 2019. Investigation of electrochemical performance of the biosynthesized α-Fe_2O_3 nanorods. Surf. Interfaces 100345.
Benzie, I.F.F., Strain, J.J., 1996. The ferric reducing ability of plasma (FRAP) as a measure of "antioxidant power": the FRAP assay. Anal. Biochem. 239, 70–76.
Bharde, A., Rautaray, D., Bansal, V., Ahmad, A., Sarkar, I., Yusuf, S.M., Sanyal, M., Sastry, M., 2006. Extracellular biosynthesis of magnetite using fungi. Small 2, 135–141.
Bhatia, S., 2016. Nanoparticles types, classification, characterization, fabrication methods and drug delivery applications. In: Natural Polymer Drug Delivery Systems. Springer International Publishing, Cham, pp. 33–93.
Bishnoi, S., Kumar, A., Selvaraj, R., 2018. Facile synthesis of magnetic iron oxide nanoparticles using inedible *Cynometra ramiflora* fruit extract waste and their photocatalytic degradation of methylene blue dye. Mater. Res. Bull. 97, 121–127.
Dhondge, S.S., Pandhurnekar, C.P., Parwate, D.V., 2010. Density, speed of sound, and refractive index of aqueous binary mixtures of some glycol ethers at T = 298.15K. J. Chem. Eng. Data 55, 3962–3968.
Edison, T.J.I., Sethuraman, M.G., 2012. Instant green synthesis of silver nanoparticles using *Terminalia chebula* fruit extract and evaluation of their catalytic activity on reduction of methylene blue. Process Biochem. 47, 1351–1357.
Ferrari, M., 2005. Cancer nanotechnology: opportunities and challenges. Nat. Rev. Cancer 5, 161–171.

G Ingale, A., 2013. Biogenic synthesis of nanoparticles and potential applications: an eco-friendly approach. J. Nanomed. Nanotechnol. 165, 1–7.
Gunarani, G.I., Raman, A.B., Dilip Kumar, J., Natarajan, S., Jegadeesan, G.B., 2019. Biogenic synthesis of Fe and NiFe nanoparticles using *Terminalia bellirica* extracts for water treatment applications. Mater. Lett. 247, 90–94.
Harshiny, M., Iswarya, C.N., Matheswaran, M., 2015. Biogenic synthesis of iron nanoparticles using *Amaranthus dubius* leaf extract as a reducing agent. Powder Technol. 286, 744–749.
Herlekar, M., Barve, S., Kumar, R., 2014. Plant-mediated green synthesis of iron nanoparticles. J. Nanoparticles 1–9, 2014.
Ibraheem, F., Aziz, M.H., Fatima, M., Shaheen, F., Ali, S.M., Huang, Q., 2019. In vitro {Cytotoxicity}, {MMP} and {ROS} activity of green synthesized nickel oxide nanoparticles using extract of {Terminalia} chebula against {MCF}-7 cells. Material Letters 234, 129–133. https://doi.org/10.1016/j.matlet.2018.09.075.
Jagathesan, G., Rajiv, P., 2018. Biosynthesis and characterization of iron oxide nanoparticles using *Eichhornia crassipes* leaf extract and assessing their antibacterial activity. Biocatal. Agric. Biotechnol. 13, 90–94.
Kamran, U., Bhatti, H.N., Iqbal, M., Jamil, S., Zahid, M., 2019. Biogenic synthesis, characterization and investigation of photocatalytic and antimicrobial activity of manganese nanoparticles synthesized from *Cinnamomum verum* bark extract. J. Mol. Struct. 1179, 532–539.
Katata-Seru, L., Moremedi, T., Aremu, O.S., Bahadur, I., 2018. Green synthesis of iron nanoparticles using *Moringa oleifera* extracts and their applications: removal of nitrate from water and antibacterial activity against *Escherichia coli*. J. Mol. Liq. 256, 296–304.
Kharat, P.B., Chavan, A.R., Humbe, A.V., Jadhav, K.M., 2019. Evaluation of thermoacoustics parameters of $CoFe_2O_4$–ethylene glycol nanofluid using ultrasonic velocity technique. J. Mater. Sci. Mater. Electron. 30, 1175–1186.
Kumar, V., Sharma, N., Sourirajan, A., Khosla, P.K., Dev, K., 2018. Comparative evaluation of antimicrobial and antioxidant potential of ethanolic extract and its fractions of bark and leaves of *Terminalia arjuna* from north-western Himalayas, India. J. Tradit. Complement. Med. 8, 100–106.
Leena, M., Srinivasan, S., Prabhaharan, M., 2015. Evaluation of acoustical parameters and thermal conductivity of TiO_2-ethylene glycol nanofluid using ultrasonic velocity measurements. Nanotechnol. Rev. 4, 449–456.
Madhavi, V., Prasad, T.N.V.K.V., Reddy, A.V.B., Ravindra Reddy, B., Madhavi, G., 2013. Application of phytogenic zerovalent iron nanoparticles in the adsorption of hexavalent chromium. Spectrochim. Acta Part A Mol. Biomol. Spectrosc. 116, 17–25.
Makarov, V.V., Love, A.J., Sinitsyna, O.V., Makarova, S.S., Yaminsky, I.V., Taliansky, M. E., Kalinina, N.O., 2014. "Green" nanotechnologies: synthesis of metal nanoparticles using plants. Acta Naturae 6, 35–44.
Mansoori, G. a, Bastami, T.R., Ahmadpour, a, Eshaghi, Z., 2008. Chapter 2 environmental application of nanotechnology. Annu. Rev. Nano Res. 2, 1–73.
Mirza, A.U., Kareem, A., Nami, S.A.A., Khan, M.S., Rehman, S., Bhat, S.A., Mohammad, A., Nishat, N., 2018. Biogenic synthesis of iron oxide nanoparticles using *Agrewia optiva* and *Prunus persica* phyto species: characterization, antibacterial and antioxidant activity. J. Photochem. Photobiol. B Biol. 185, 262–274.
Mittal, A.K., Chisti, Y., Banerjee, U.C., 2013. Synthesis of metallic nanoparticles using plant extracts. Biotechnol. Adv. 31, 346–356.
Moon, J.-W., Rawn, C.J., Rondinone, A.J., Love, L.J., Roh, Y., Everett, S.M., Lauf, R.J., Phelps, T.J., 2010. Large-scale production of magnetic nanoparticles using bacterial fermentation. J. Ind. Microbiol. Biotechnol. 37, 1023–1031.
Muthukumar, H., Matheswaran, M., 2015. Amaranthus spinosus leaf extract mediated FeO nanoparticles: physicochemical traits, photocatalytic and antioxidant activity. ACS Sustain. Chem. Eng. 3, 3149–3156. https://doi.org/10.1021/acssuschemeng.5b00722.
Nabeel Rashin, M., Hemalatha, J., 2014. A novel ultrasonic approach to determine thermal conductivity in CuO–ethylene glycol nanofluids. J. Mol. Liq. 197, 257–262.
Nandhini, N.T., Rajeshkumar, S., Mythili, S., 2019. The possible mechanism of eco-friendly synthesized nanoparticles on hazardous dyes degradation. Biocatal. Agric. Biotechnol. 19, 101–138.
Naseem, T., Farrukh, M.A., 2015. Antibacterial activity of green synthesis of iron nanoparticles using *Lawsonia inermis* and *Gardenia jasminoides* leaves extract. J. Chem. 1–7, 2015.
Pastoriza-Gallego, M.J., Lugo, L., Legido, J.L., Piñeiro, M.M., 2011. Enhancement of thermal conductivity and volumetric behavior of FexOy nanofluids. J. Appl. Phys. 1, 110–114.
Pfundstein, B., El Desouky, S.K., Hull, W.E., Haubner, R., Erben, G., Owen, R.W., 2010. Polyphenolic compounds in the fruits of Egyptian medicinal plants (*Terminalia bellerica, Terminalia chebula and Terminalia horrida*): characterization, quantitation and determination of antioxidant capacities. Phytochemistry 71, 1132–1148.
Qu, X., Alvarez, P.J.J., Li, Q., 2013. Applications of nanotechnology in water and wastewater treatment. Water Res. 47, 3931–3946.
Radini, I.A., Hasan, N., Malik, M.A., Khan, Z., 2018. Biosynthesis of iron nanoparticles using Trigonella foenum-graecum seed extract for photocatalytic methyl orange dye degradation and antibacterial applications. J. Photochem. Photobiol. B Biol. 183, 154–163.
Rajiv, P., Bavadharani, B., Kumar, M.N., Vanathi, P., 2017. Synthesis and characterization of biogenic iron oxide nanoparticles using green chemistry approach and evaluating their biological activities. Biocatal. Agric. Biotechnol. 12, 45–49.
Saeed, N., Khan, M.R., Shabbir, M., 2012. Antioxidant activity, total phenolic and total flavonoid contents of whole plant extracts *Torilis leptophylla L.* BMC Complement Altern. Med. 12, 1174.
Sahoo, J.K., Paikra, S.K., Mishra, M., Sahoo, H., 2019. Amine functionalized magnetic iron oxide nanoparticles: synthesis, antibacterial activity and rapid removal of Congo red dye. J. Mol. Liq. 282, 428–440.
Saif, S., Tahir, A., Chen, Y., 2016. Green synthesis of iron nanoparticles and their environmental applications and implications. Nanomaterials 6, 209–215.
Schröfel, A., Kratošová, G., Šafařík, I., Šafaříková, M., Raška, I., Shor, L.M., 2014. Applications of biosynthesized metallic nanoparticles - a review. Acta Biomater. 10, 4023–4042.
Sharma, V.K., Sayes, C.M., Guo, B., Pillai, S., Parsons, J.G., Wang, C., Yan, B., Ma, X., 2019. Interactions between silver nanoparticles and other metal nanoparticles under environmentally relevant conditions: a review. Sci. Total Environ. 653, 1042–1051.
Singleton, V.L., Orthofer, R., Lamuela-Raventós, R.M., 1999. Analysis of total phenols and other oxidation substrates and antioxidants by means of folin-ciocalteu reagent. In: Methods in Enzymology. Elsevier, pp. 152–178.
Sivamaruthi, B.S., Ramkumar, V.S., Archunan, G., Chaiyasut, C., Suganthy, N., 2019. iogenic synthesis of silver palladium bimetallic nanoparticles from fruit extract of Terminalia chebula – In vitro evaluation of anticancer and antimicrobial activity. J. Drug Deliv. Sci. Technol 51, 139–151. https://doi.org/10.1016/j.jddst.2019.02.024.
Sneha, U., Karthikeyan, R., 2019. Bactericidal activity of ayurvedic formulation against cariogenic microorganisms. Biocatal. Agric. Biotechnol. 18, 101026.
Subramaniyam, V., Subashchandrabose, S.R., Thavamani, P., Megharaj, M., Chen, Z., Naidu, R., 2015. *Chlorococcum sp. MM11*—a novel phyco-nanofactory for the synthesis of iron nanoparticles. J. Appl. Phycol. 27, 1861–1869.
Vasantharaj, S., Sathiyavimal, S., Senthilkumar, P., LewisOscar, F., Pugazhendhi, A., 2019. Biosynthesis of iron oxide nanoparticles using leaf extract of *Ruellia tuberosa*: antimicrobial properties and their applications in photocatalytic degradation. J. Photochem. Photobiol. B Biol. 192, 74–82.
Vaseghi, Z., Nematollahzadeh, A., Tavakoli, O., 2017. Green methods for the synthesis of metal nanoparticles using biogenic reducing agents: a review. Rev. Chem. Eng. 34, 529–560.
Vijayaraghavan, K., Ashokkumar, T., 2017. Plant-mediated biosynthesis of metallic nanoparticles: a review of literature, factors affecting synthesis, characterization techniques and applications. J. Environ. Chem. Eng. 6, 4866–4883.
Wang, T., Jin, X., Chen, Z., Megharaj, M., Naidu, R., 2014. Green synthesis of Fe nanoparticles using eucalyptus leaf extracts for treatment of eutrophic wastewater. Sci. Total Environ. 466–467, 210–213.
Wiesner, M.R., Lowry, G.V., Alvarez, P., Dionysiou, D., Biswas, P., 2006. Assessing the risks of manufactured nanomaterials. Environ. Sci. Technol. 40, 4336–4345.